Applied Energy 108 (2013) 477–485

Contents lists available at SciVerse ScienceDirect

Applied Energy

journal homepage: www.elsevier.com/locate/apenergy

Bubble dissolution in horizontal turbulent bubbly flow in domestic central heating system

Y.T. Ge [a,*], A.M. Fsadni [a], H.S. Wang [b]

[a] Mechanical Engineering, School of Engineering and Design, Brunel University, Uxbridge, Middlesex UB8 3PH, UK
[b] School of Engineering and Materials Science, Queen Mary University of London, Mile End Road, London E1 4NS, UK

HIGHLIGHTS

- Experimental study on the bubble dissolution inside horizontal pipes.
- The dissolution rates measured for bubble size ratios are within 12% per second.
- The effect parameters on dissolution rates are investigated.
- The bubble dissolution model has been developed.

ARTICLE INFO

Article history:
Received 13 August 2012
Received in revised form 14 February 2013
Accepted 23 March 2013
Available online 18 April 2013

Keywords:
Bubble dissolution
Horizontal bubbly flow
Central heating systems
Experiment
Modelling

ABSTRACT

In a domestic central heating system, the phenomenon of microbubble nucleation and detachment on the surface of a boiler heat exchanger finds its origins in the high surface temperature of the wall and consequential localised super saturation conditions. If the surrounding bulk fluid is at under-saturated conditions, then after exiting the boiler, the occurrence is followed by bubbly flow and bubble dissolution. A comprehensive understanding of the fundamentals of bubble dissolution in such a domestic wet central heating system is essential for an enhanced deaeration technique that would consequently improve system performance. In this paper, the bubble dissolution rate along a horizontal pipe was investigated experimentally at different operating conditions in a purpose built test rig of a standard domestic central heating system. A high speed camera was used to measure the bubble size at different depths of focal plane using two square sectioned sight glasses at two stations, spaced 2.2 m apart. A dynamic model for bubble dissolution in horizontal bubbly flow has been developed and compared with experimental data. The effects of several important operating and structural parameters such as saturation ratio, velocity, temperature, pressure of the bulk liquid flow, initial bubble size and pipe inside diameter on the bubble dissolution were thus examined using the model. This model provides a useful tool for understanding bubble behaviours in central heating systems and optimising the system efficiency.

1. Introduction

The generation of microbubbles under super saturated conditions in a closed system is a common phenomenon subsisting in major industrial and energy processes including those of chemical, pharmaceutical, food, heating (Joelsson and Gustavsson [1]), renewable energy (Chen and Yang [2]) or power generation (Wang et al. [3]). The appearance of a secondary bubble phase is mostly undesirable due to its negative effects on system performance. For example, in a domestic wet central heating system, the occurrence of microbubbles could result in cavitations' corrosion, unwanted noise, blockages and inefficient performance due to radiator cold spots. Hence, the lifetime of dissolving bubbles, droplets, and solid particles in an isothermal bulk phase is a major consideration in the design of equipment in a variety of industrial applications.

Microbubbles in a domestic wet central heating system nucleate on the surface of the primary heat exchanger due to elevated wall temperatures, thereby resulting in super saturation or near super saturated conditions in the vicinity of the wall. It is known from experimental results that the bubble nucleation rates range between 0.3 and 4 bubbles per cm^2 per second and the mean bubble diameters at the boiler exit vary from 0.13 to 0.39 mm (Fsadni et al. [4]). In addition, under most operating conditions the water in the system pipe work is at under-saturated conditions. Hence, the highest bubble density is found at the immediate exit of the boiler, and consequently, the average bubble diameter and density are expected to decrease with the distance from the boiler unit as mass transfer through dissolution takes place. Passive deaerators

* Corresponding author. Tel.: +44 1895 266722; fax: +44 1895 256392.
E-mail address: yunting.ge@brunel.ac.uk (Y.T. Ge).

0306-2619/$ - see front matter © 2013 Elsevier Ltd. All rights reserved.
http://dx.doi.org/10.1016/j.apenergy.2013.03.055

Nomenclature

C	gas concentration (kg/m^3)
D_b	bubble diameter (mm)
d_h	hydraulic diameter (mm)
D_g	gas diffusivity (m^2/s)
d_i	inside diameter of pipe (mm)
m_b	specific mass flux on the bubble boundary (kg/m^2 s)
P	pressure (bar)
R	radius of the bubble (m)
R_i	radius of the bubble at station HSG1 (mm)
R_1	radius of the bubble at station HSG1 (mm)
R_2	radius of the bubble at station HSG2 (mm)
Re	Reynolds number, $U_f d/v$
s	depth of sight glass focal plane measured vertically downwards from the top plane of the sight glass (mm)
Sc	Schmidt number, v/D_g
Sh	Sherwood number, $\beta D_b/D_g$
T	time (s)
Δt	time interval (s)
T_f	bulk fluid temperature (°C)
U_f	bulk fluid velocity (m/s)
X^T	gas solubility factor (m^3/kg bar)

Greek symbols

α	saturation ratio
ε	bubble size ration R_2/R_1
β	mass transfer coefficient (m/s)
v	kinematic viscosity of liquid (m^2/s)
ρ	density of liquid (kg/m^3)

Subscripts

1	at horizontal sight glass (HSG1), see Fig. 1
2	at horizontal sight glass (HSG2), see Fig. 1
ave	average
b	bubble, bulk
f	fluid
Exp	experimental
g	gas in bubble
gas	gas in the central heating system
i	inner, initial
Pre	predicted
R	bubble boundary with radius R
sat	saturation, maximum

are installed at the flow line of the boiler so as to capture bubbles, thus ensuring that the dissolved air content in the system water is reduced, consequently reducing the saturation ratio and the nucleation rate at the heat exchanger wall. Therefore, a comprehensive analysis of the expected rate of dissolution for the bubbles present in such a system is considered as essential for the optimal positioning of such a device.

From public literature, the bubble dissolutions due to gas diffusion at under-saturated conditions have been extensively studied but are mostly based on theoretical analysis. Kress and Keyes [5] investigated and quantified the liquid phase controlled mass transfer to bubbles in co-current turbulent pipe flow using an empirical correlation to calculate mass transfer coefficients. They reported that data obtained for the mass transfer in agitated vessels could not be directly used to predict mass transfer in pipeline flow, as lower mass transfer rates were expected in agitated vessels due to the relative ineffectiveness of the turbulence. Lezhnin et al. [6] examined the dissolution of air bubbles in water flowing in a horizontal pipeline, where in contrast to the nearly constant pressure used in the present study, the pressure dropped from several bars to atmospheric. They therefore classified the mass transfer mechanism in under-saturated bubbly flow as turbulent diffusion. Other studies by Hesketh et al. [7] and Martínez-Bazán et al. [8] investigated the bubble breakup in turbulent pipe flow. However, the effect of such a phenomenon is considered minimal for the conditions of the present study, due to the small bubble diameters and quasi-spherical bubble shape characterising such systems (Fsadni et al. [4]). Most studies on bubble dissolution in under-saturated solutions have been done for isolated gas bubbles and were based on the Epstein and Plesset [9] gas diffusion model such as Duda and Vrentas [10] and Cable and Frade [11]. These studies found their origin as a result of a direct interest in the dynamics of bubble dissolution or in the need to obtain a value for the diffusivity of the gas in a liquid with a known solubility. The theoretical interpretation of these experiments has been based on the consideration of an isolated sphere in spherically symmetrical conditions. Hence, at under-saturated conditions, the bubble dissolves at a rate controlled by the diffusion of gas through the liquid. Similarly, the bubble growth rate at supersaturated conditions is also dependent on the diffusion of gas through the liquid. These bubble growth and condensation rates have been investigated in boiling and subcooled flow boiling conditions, whereby models have been developed to predict the ratio of the actual to maximum bubble diameters at pre-determined time intervals by Prodanovic et al. [12] and Akiyama and Tachibana [13]. On the other hand, a number of adaptations have been developed for the symmetrically isolated bubble model. However, such adaptations require correlations in order to compensate for the imperfect bubble spherical shape and diffusion field. Similar adaptations have been done for the dissolution of microbubbles attached to a wall under flow conditions by Cable [14] and Kentish et al. [15]. Such models have also been adapted in medical science involving the analysis of gas bubble dissolution in whole blood and plasma by Yang et al. [16].

So far few experimental data directly related to bubble dissolution in central heating or associated systems are available. Moreover, limited attention in literature, to date, has been paid to the expected dissolution of free bubbles in turbulent flow with minimal slip.

In this paper, the bubble dissolution in horizontal turbulent bubbly flow has been examined experimentally in a test rig of domestic central heating system. A high speed camera is used to measure and record the bubble sizes across two separate pipe sections at different operating states. A dynamic bubble dissolution model is developed and compared with the measurements. The model is therefore utilised as an efficient design and analysis tool to predict the effects of fluid saturation ratio, velocity, temperature, pressure and initial bubble size on the bubble dissolution rate, which are significant factors in the understanding of bubbly behaviours in domestic central heating systems.

2. Experimental set-up and procedure

A schematic layout of the experimental test rig is shown in Fig. 1. A Commercial condensing boiler is connected to a 22 mm diameter (outer) copper pipe work consisting of a radiator and a buffer vessel. The condensing boiler is used since it is mandatory equipment for new buildings in most European Union member states (Semmens and Ahmed [17]) due to its high efficiency and consequently energy saving properties (Chen et al. [18]). The boiler

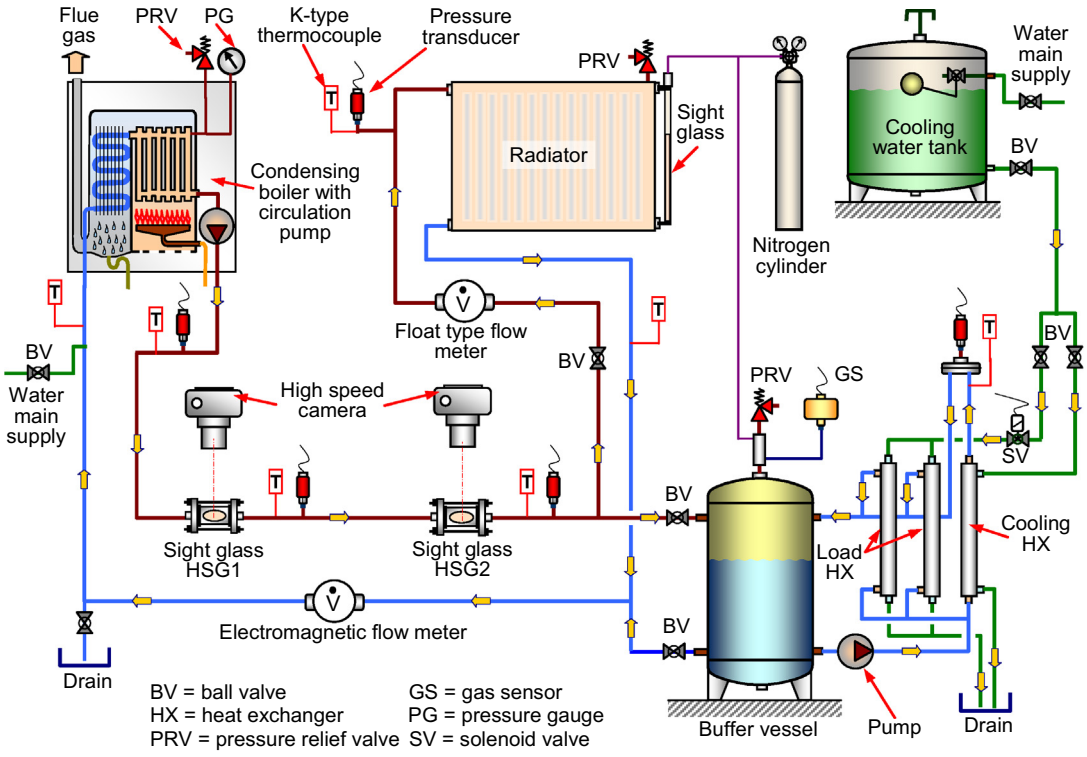

Fig. 1. Test rig of domestic central heating system.

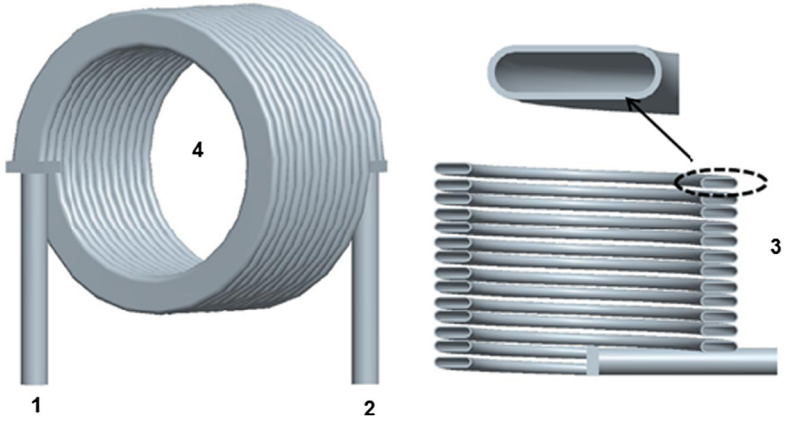

1 Water inlet
2 Water outlet
3 Sectional view of heating tubes - d_h = 7.9 mm
4 Location of gas fired burner

Fig. 2. Primary heat exchanger assembly and cross-sectional view of the rectangular tube.

heat exchanger design used in the current study consists of 12 rectangular tubes coiled around the boiler burner in a helical structure, as shown in Fig. 2. The first 4 tubes at the return end are compartmentalised into a condenser where the flue gases from the gas burner condense on the cold tube surfaces, releasing latent heat, consequently resulting in higher efficiencies. At the inlet, the system mass flow rate is split in half and channelled into two parallel tubes in the helical structure. Therefore, the system mass flow rate is equal to twice that observed in the boiler tubes. At the boiler exit, two identical square sight glasses HSG1 and HSG2, each with internal dimensions of 20×20 mm, were installed for filming microbubbles at two stations, spaced 2.2 m apart, on a horizontal straight line pipe. Along the pipe work circuit, seven stainless steel sheathed K type thermocouples are used to measure the fluid temperatures and four pressure transducers used to monitor the system pressure at different locations. The fifth pressure transducer, in combination with a semi-permeable silicone membrane, is used to monitor the dissolved gas partial pressure. A tap water cooling heat exchanger is used to cool the system water to a lower temperature of between 20 and 45 °C, to allow the partial gas pressure monitoring system to function as required.

The system fluid flow rate is monitored through an Electromag 500 Series electromagnetic flow metre. A National Instruments cDAQ-9172 chassis and relevant data modules receives all the signals from the pressure transducers, thermocouples and electromagnetic flow metre. The signals are then managed through the use of a block diagram set up on LabVIEW which transfers the saved data onto Excel files. These thermocouples and pressure

transducers and the LabVIEW system were calibrated using standard calibrating equipment.

It should be noted that standard central heating systems make use of untreated steel radiators and copper piping. These radiators result in limited oxidation due to a presence of dissolved oxygen in the tap water. The oxidation process releases iron oxide and hydrogen gas, and leaves nitrogen as the dominant dissolved gas. Nitrogen is therefore considered as the sole nucleated and dissolved gas within the system.

The system pressure was set at 2.7 bar for all experimental runs using a nitrogen gas cylinder connected to a standard cylinder regulator. As illustrated in Fig. 1 this was done through a one-way valve at the top of the radiator. Nitrogen gas was used as it is known to be the predominant dissolved gas in wet central heating systems, as mentioned above. The system heating load was set through the control of the boiler return temperature that was maintained at a constant level through the use of a magnetic tap connected to the tap water mains supply line.

The analysis of dissolved gases, through the use of Orbisphere 3655 oxygen and Orbisphere 3654 hydrogen sensors, was able to measure a very low concentration of oxygen and hydrogen present in their dissolved form. In fact, both gases were present in concentrations of ca. 9 PPB. This is in line with the findings reported by studies done in industry, through long term experimentation with domestic central heating test rigs. In fact, oxygen, methane and carbon dioxide concentrations were found to make up to 3% of the volume of the gases present at the top of a radiator. Therefore, nitrogen is evidently the dominant gas and its dissolved gas properties are used in this present study. The partial gas pressure was calculated by subtracting the vapour pressure from the gas transducer reading, as defined by Lubetkin and Blackwell [20]. The actual gas concentration in the system C_{gas} was calculated using nitrogen gas solubility data provided by Battino [21] and Henry's law of Eq. (1) (Gerrard [22]).

$$C_{gas} = P_g X^T \tag{1}$$

where P_g is the partial pressure of the dissolved gas, and X^T is the gas solubility factor. The saturation ratio α was calculated by Eq. (2) as defined by Jones et al. [19].

$$\alpha = C_{gas}/C_{sat} \tag{2}$$

where C_{sat} is the maximum gas concentration at the bulk fluid conditions (standard cm^3/L water).

To investigate the bubble dissolutions at different operating conditions, two sets of the system parameters, as listed in Table 1, were controlled during experiments following the procedures below:

(i) Under saturation conditions were achieved through the sudden release in system pressure followed by a subsequent re-pressurisation. Saturation ratios close to unity were attained through the filling of the upper part of the radiator with a head of nitrogen gas. System saturation ratios in the pipe work were set between 0.89 and 0.97, as defined by Jones et al. [19] and calculated using Eq. (2).
(ii) The system flow rate or velocity was stepped up using a ball valve on the supply line from a minimum 0.25 m/s to a maximum of 0.52 m/s. This is equivalent to a system flow rate ranging from 6 to 12.5 L/min.

2.1. Imaging and analysis

As illustrated in Figs. 3 and 4, a square section of the horizontal sight glass (HSG1, HSG2) was designed to reduce the distortion as a result of viewing bubbles through a curved surface. As discussed by Prodanovic et al. [12], such distortions are due to light refraction. A Vision Research Phantom V5 high speed camera connected to a PC was used to film and store the video clips as illustrated in Fig. 3. A monozoom (Navitar) microscope lens was used to develop the desired magnification.

Table 1
Experimental conditions.

Test	d_i (mm)	R_i (mm)	P (bar)	T_f (°C)	U_f (m/s)	α-
i	20	0.066–0.096	2.7	74.5	0.52	0.89–0.97
ii	20	0.074–0.135	2.7	80.0	0.25–0.52	0.89

The experiment implemented a shutter speed of 30 μs and a frame speed of 100 frames per second. Lighting was provided by two high intensity 60 W light sources attached to semi rigid fibre optic light guides. The system was calibrated using a number of standard sized gauges and subsequent scaling. A frame size was attained at 5.62 mm × 5.62 mm and the depth of field was limited to approximately 1.5 mm.

This depth of field was determined through use of a precision vertical movement rack which determines points at which a number of pre-defined objects are in and out of focus with the measured vertical movement of the camera. Five focal planes were used, being at 0, 4, 8, 12 and 16 mm from the top plane of the sight glass. This was necessary so as to analyse the bubble distribution across the horizontal pipe work.

The video films were converted to image frames saved as 'tag image file format' or tiff files using the Phantom Version 606 camera software. Image analysis was done through use of the software, Image-Pro Plus. A macro was written enabling a series of images to be analysed for in-focus bubble counts and diameters. The macro included the use of a Sobel filter to enable the distinction between in and out of focus bubbles. The Sobel filter plots the gradient of intensity change between objects and their background through the extraction and enhancement of edges and contours. This is done by expressing intensity differences or gradients between neighbouring pixels as an intensity value. Therefore, objects that are in focus have sharp edges with a high gradient change which consequently results in high intensity values, whereas out of focus objects do not display such a characteristic. The Sobel filter was used as it is less sensitive to image noise as compared to other filtering techniques (Image-Pro [23]). A typical analysed image is illustrated in Fig. 5, where in focus bubbles are circled.

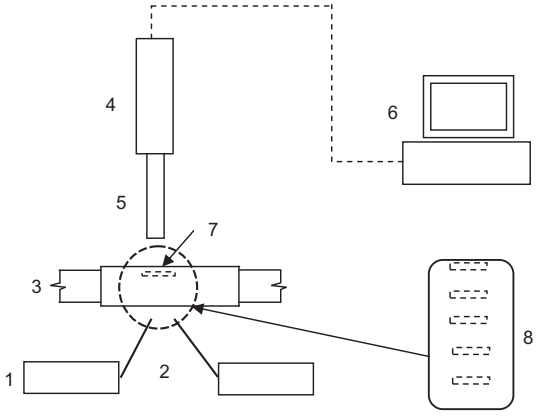

1 Light sources
2 Fibre optic light guide
3 Square sight glass section (20 mm × 20 mm)
4 High speed camera
5 Microscope lens
6 PC wired to camera
7 Focal depth of 1.5 mm
8 Top view of sight glass focal planes at 0, 4, 8, 12, 16 mm

Fig. 3. Bubble size measurement equipment.

Fig. 4. Camera and sight glass set up.

2.2. Uncertainty analysis

The main errors of this study originate from the limitations of the video images due to the presence of in and out of focus bubbles. Illumination shadowing and manual measurement errors are also considered as potential errors. These errors are mostly due to the precision with which the macro based image analysis software could determine the in-focus bubbles from the out of focus ones. A manual analysis of sample images has shown an average accuracy of ±10% in determining between in and out of focus bubbles. This error value is an estimate as a manual analysis of in and out of focus bubbles is considered to be subjective due to the lack of a set of fixed parameters for the manual selection. The volumetric void fraction was calculated through the use of the Coleman and Steel method [24]. Other errors are due to the flow metre which has an accuracy of 0.5% whereas pressure transducers have an accuracy of 0.3%. The stainless steel sheathed K type thermocouples have an accuracy of ±0.1 K. The effects of these errors are considered to be minimal for the measurement requirements of the present study. The experimental uncertainties of the saturation ratio α at bulk fluid conditions, the bubble size ratio ε and the volumetric void fraction were estimated to be within ±1.9%, ±7.1% and ±11.7%, respectively.

3. Experimental results and comparison with bubble dissolution model

The recorded experimental results for test conditions (i) and (ii) as listed in Table 1 will be explained and compared with a developed model for bubble dissolution in the following sections. This model is applied to analyse the effecting parameters on bubble dissolution behaviours.

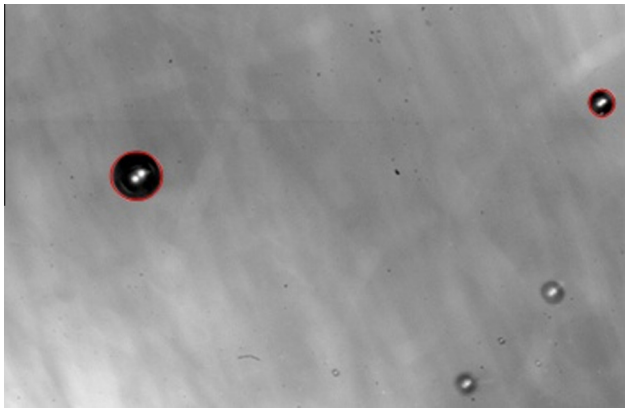

Fig. 5. Typical photograph. Post processing with in focus bubbles circled.

3.1. Development of bubble dissolution model

To explore the bubble dissolution behaviours of bubbly flow in a horizontal pipe within a domestic central heating system, a dynamic model has been developed based on the mechanism of turbulent diffusion with the following assumptions:

(1) The liquid fluid is pure water and the flow is isothermal (due to good insulation between HSG1 and HSG2) along the horizontal pipe.
(2) The relative velocity between the bubble and surrounding liquid flow is negligible.
(3) The effect of bubble surface tension on the gas diffusivity is considered minimal.
(4) The liquid fluid at the bubble boundary is at a saturated state.
(5) The gas inside the bubble i.e. pure Nitrogen is the ideal gas.
(6) The bubble is spherical between HSG1 and HSG2.

The mass flux of the gas m_b from a flowing bubble to ambient liquid flow can be calculated as:

$$m_b = \beta(C_R - C_f) \tag{3}$$

where C_R is the gas concentration when the radius of the bubble is R, C_f is the gas concentration in the surrounding fluid of the bubble, β is the mass transfer coefficient. Three empirical correlations below may be used to calculate β ($=ShD_g/D_b$):

Kress and Keyes [5]

$$Sh = 0.34\frac{D_b}{d_i}Re^{0.94}Sc^{0.5} \tag{4}$$

Avdeev [25]

$$Sh = 0.228\frac{D_b}{d_i}Re^{0.7}Sc^{0.5} \tag{5}$$

and Kawase et al. [26]

$$Sh = 0.38\frac{D_b}{d_i}Re^{0.75}Sc^{0.5} \tag{6}$$

It should be noted that Eq. (4) was obtained from experimental results on the bubble mass transfer in a horizontal pipeline with Reynolds number (Re) range from 1.2×10^4 to 2×10^5 and Schmidt number (Sc) from 370 to 2013, which are close to the conditions of the present study in term of Re number. However, due to its higher exponent value on the Reynolds number, the turbulent effect on bubble dissolution is more significant than those of Eqs. (5) and (6). For Eq. (5), it was based on the operating conditions with Reynolds number (Re) range from 8×10^3 to 2×10^6, Prandtl (Pr) number from .083 to 568 and pressure up to 10 MPa. As to Eq. (6), the applicable ranges of Re and Sc or Pr were not given explicitly. Instead, it was correlated with water fluid for bubble column diameter from 0.14 m to 7.62 m, fluid viscosity from 0.00081 Pa s to 0.01303 Pa s, and superficial gas velocity from 0.01 m/s to 0.075 m/s.

The mass conservation equation of a bubble in bubbly flow at under or super saturated fluid conditions can be written as:

$$\rho_g\frac{dR}{dt} + \frac{R}{3}\frac{d\rho_g}{dt} = -m_b \tag{7}$$

Assuming thermodynamic equilibrium at the boundary of the bubble, Henry's law of Eq. (1) can be used to calculate C_R in Eq. (3) at the process of bubble dissolution.

Substituting Eq. (3) into Eq. (7) yields:

$$\rho_g \frac{dR}{dt} + \frac{R}{3}\frac{d\rho_g}{dt} = -\beta(C_R - C_f) \tag{8}$$

Eq. (8) is then discretized at a small time interval Δt as Eq. (9) below, such that the temporal variation of bubble dissolution rate can be solved.

$$\rho_g(t)\frac{R(t+\Delta t)-R(t)}{\Delta t} + \frac{R(t)}{3}\frac{\rho_g(t+\Delta t)-\rho_g(t)}{\Delta t} = -\beta[C_R(t) - C_f(t)] \tag{9}$$

3.2. Comparison of experimental data and model predictions

Using Eqs. (4)–(6) to calculate the mass transfer coefficient β under the operating conditions given in Table 1, the predictions by the new model are compared with the present experimental data.

At the test conditions (i) and (ii) listed in Table 1 and Fig. 6 shows the bubble size ratio ε measured between HSG2 and HSG1 for different depths of the sight glass focal plane. It should be noted that the radii of the bubble R_1 and R_2 were measured at HSG1 and HSG2, respectively, at the same depth of the sight glass focal plane, assuming that the same bubble flowing from one location to another does not mix. No appreciable relation is observable between the bubble size ratio ε and the depth of the sight glass focal plane considering the uncertainty of image taking and processing. The measured ε decreases with an increasing fluid saturation ratio due to the effect of the gas density difference on mass transfer (see Fig. 6a). The gas dissolution is greater for higher bulk fluid velocities as expected (see Fig. 6b). On the other hand, however, the gas dissolution decreases with a higher bulk fluid velocity because the time for the bubble to travel between the two fixed locations i.e. HSG1 and HSG2 is shortened. Therefore, the effect of bulk fluid velocity on the bubble dissolution rate is not clearly revealed from the measurements. The predicted values of ε by the model using Eq. (4) to calculate β are also shown in Fig. 6, in which the model shows the same trend as that of the measured data but significantly under predicts the bubble size ratios.

Similarly, Figs. 7 and 8 show respectively the predicted values of ε by the model using Eqs. (5) and (6). From Figs. 7 and 8, it can be seen that the model using Eqs. (5) and (6) to calculate β each give the same trend as the measured data but both significantly over predict the bubble size ratios.

As mentioned above, Eq. (4) was based on the data obtained under the experimental conditions similar to the present study. However, the model using Eq. (4) to calculate β greatly under predicts the bubble size ratio. To match the present experimental data, a new correlation, taking the same form of Eq. (4) was then obtained by an optimised fitting of the model and the experimental data. Taking the same exponent of *Sc* number 0.5 and the leading coefficient 0.34, the exponent of the Reynolds number is correlated as 0.86, and the new correlation of *Sh* number is therefore revised as:

$$Sh = 0.34\frac{D_b}{d_i}Re^{0.86}Sc^{0.5} \tag{10}$$

As expected, Eq. (10) gives good agreement with all the experimental data obtained under conditions (i) and (ii) as shown in Fig. 9. Consequently, the discrepancy of the model prediction from the experimental results is mostly within 10%, as shown in Fig. 10. Considering the actual operating conditions and pipe sizes of conven-

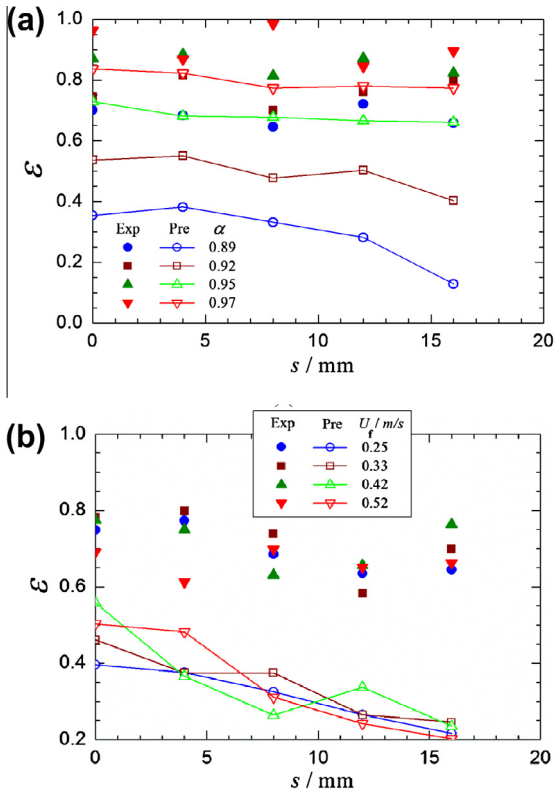

Fig. 6. Variations of predicted and measured bubble size ratio with the depth of the sight glass focal plane for: (a) different saturation ratios, test condition (i) given in Table 1; (b) different bulk fluid velocity, test condition (ii) given in Table 1. Eq. (4) is used to calculate β in the model. The solid line is a guide for the eye.

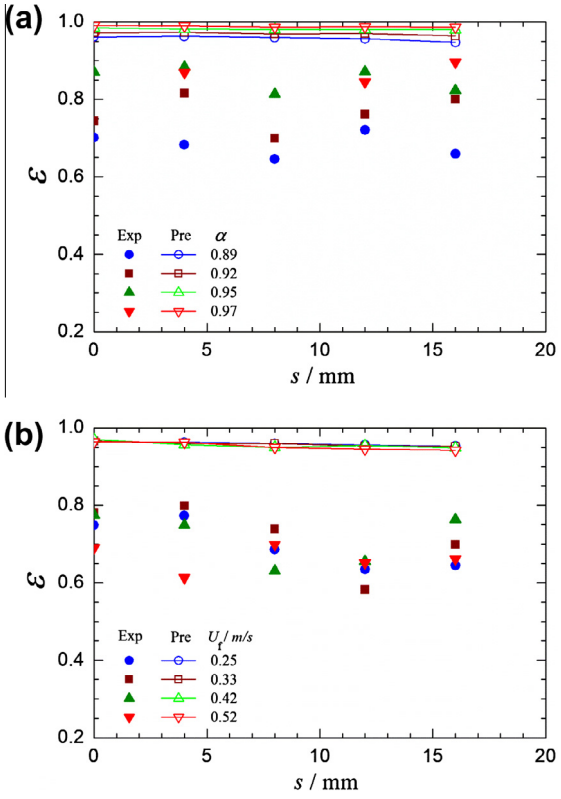

Fig. 7. Variations of predicted and measured bubble size ratio with the depth of the sight glass focal plane for: (a) different saturation ratios, test condition (i) given in Table 1; (b) different bulk fluid velocity, test condition (ii) given in Table 1. Eq. (5) is used to calculate β in the model. The solid line is a guide for the eye.

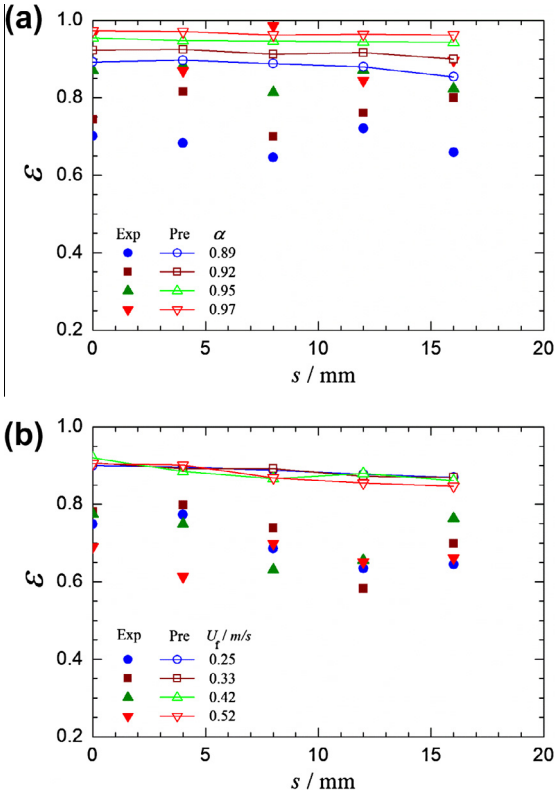

Fig. 8. Variations of predicted and measured bubble size ratio with the depth of the sight glass focal plane for: (a) different saturation ratios, test condition (i) given in Table 1; (b) different bulk fluid velocity, test condition (ii) given in Table 1. Eq. (6) is used to calculate β in the model. The solid line is a guide for the eye.

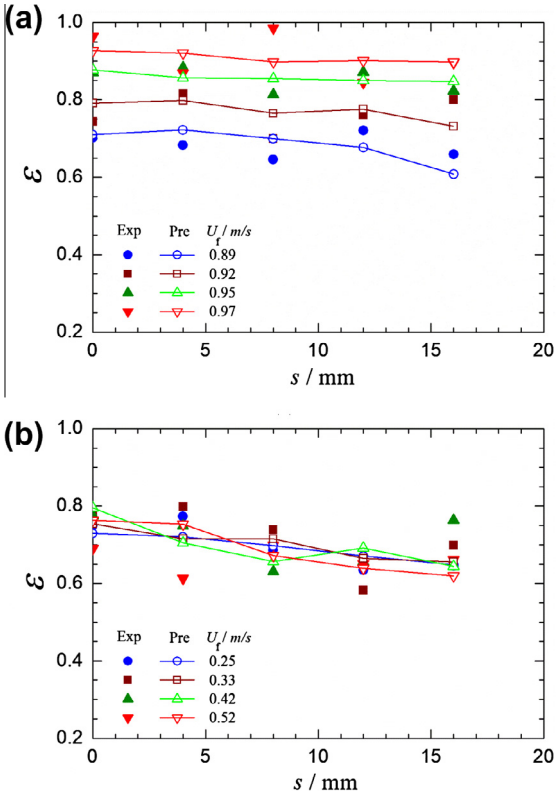

Fig. 9. Variations of predicted and measured bubble size ratio with the depth of the sight glass focal plane for: (a) different saturation ratios, test condition (i) given in Table 1; (b) different bulk fluid velocity, test condition (ii) given in Table 1. Eq. (4) is used to calculate β in the model. The solid line is a guide for the eye.

tional domestic central heating systems, for correlation (10), the applicable range of Re is from 9.0×10^3 to 5.4×10^4 and Sc from 50 to 90. These application ranges although are much slimmer than those in correlations (4)–(6), the new correlation is more accurate and quite suitable for the analysis of bubble behaviours in domestic central heating systems.

To clearly examine the effects of the saturation ratio α and bulk fluid velocity U_f on the bubble size ratio ε, the values of ε from measurements and predictions are averaged along all the depths of sight glass focal plane for both test conditions (i) and (ii) given in Table 1. The variations of the averaged ε with the saturation ratio α and bulk fluid velocity U_f are depicted in Figs. 11 and 12 respectively. From both the experimental data and predictions, we can see that at test condition (i), the averaged ε increases almost linearly with increasing saturation ration α. However, for the same reason mentioned above, the effect of bulk fluid velocity on the average ε is not appreciable from the averaged measurement and predicted results shown in Fig. 12.

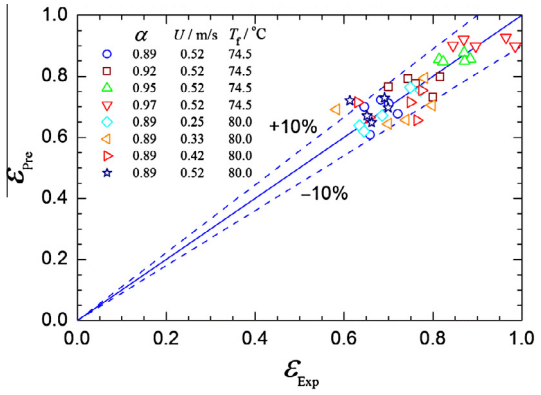

Fig. 10. Comparison of predicted and measured bubble size ratio using the new model (Eq. (10) to calculate β).

4. Parametric study

The new model is then used to study the effects of fluid velocity, saturation ratio, fluid temperature and pressure, bubble initial size and inner diameter of the pipe on the bubble dissolution rate i.e. ε. To ensure a fair comparison and justified conclusions for all the following simulations, ε is calculated based on a fixed bubble travelling time of 5 s instead of a fixed flowing distance as stated in Section 3.

Fig. 13 plots the predicted values of ε as a function of fluid velocity. The pipe inner diameter, fluid temperature, fluid pressure and bubble initial radius are kept constant at 20 mm, 80 °C, 3 bar and 0.2 mm, respectively. When the fluid is under-saturated ($\alpha < 1$), ε decreases with increasing fluid velocity since the enhanced turbulent flow results in an augmented bubble dissolution. For a given fluid velocity, ε increases with increasing α until α reaches unity. This is because the elevated α actually diminishes the gas mass transfer potential between the gas inside the bubble and surrounding liquid. Whilst the fluid is at super-saturated conditions ($\alpha > 1$), for the same reason, the higher α and fluid velocity enhance the bubble size enlarge rate despite ε being effectively increased due to the gas mass transfer in the opposite direction. It should be noted that the relationship between ε and fluid velocity for a constant α is almost linear since the fluid temperature and pressure during the bubble dissolution or increase process both remain relatively stable such that only the mass transfer coefficients are altered with limited fluid velocity changes.

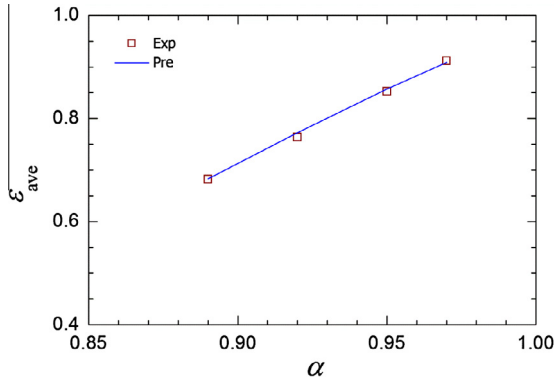

Fig. 11. Variation of predicted and measured bubble size ratio with liquid saturation ratio. Test condition (i) given in Table 1.

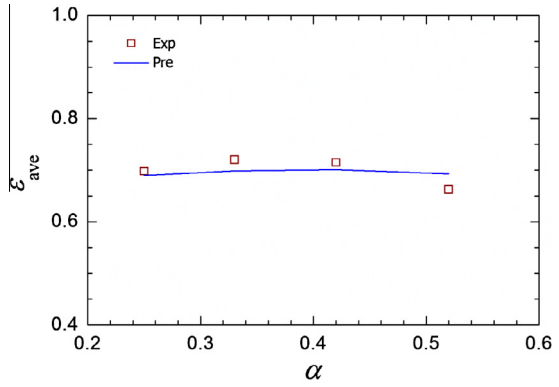

Fig. 12. Variation of predicted and measured bubble size ratio with bulk fluid velocity. Test condition (ii) given in Table 1.

Fig. 14 shows the variations of ε with fluid pressure for different fluid temperatures. The pipe inner diameter, initial saturation ratio, fluid velocity and initial bubble radius are constant at 20 mm, 0.8, 0.8 m/s and 0.2 mm, respectively. At constant fluid temperatures, ε decreases with increasing fluid pressure and this diminishing rate is more significant at elevated fluid temperatures. However, the variations of ε with fluid temperatures at constant pressure are not monotonous but instead determined by the fluid pressure magnitude. When the pressure is below a specific value (roughly 2.7 bar), the value of ε is higher for greater fluid temperatures. These can be explained with the fundamental Henry's law that at a constant fluid temperature, the gas solubility increases, thus bubble size reduces with higher pressures and the higher fluid temperature simultaneously causes the solubility to drop and the bubble size to enlarge. However, if the pressure variation is larger, the effect of fluid pressure on ε overtakes that of the fluid temperature.

Fig. 15 shows the variations of predicted values of ε with the initial bubble radius for different inner diameters of the pipe. The initial saturation ratio, fluid velocity, fluid temperature and fluid pressure are constant at 0.9, 0.8 m/s, 80 °C and 3 bar, respectively. For a constant pipe inner diameter, ε increases significantly when the initial bubble size is less than about 0.2 mm and more slowly when the initial bubble size is greater than the same value. Conversely, the effect of the pipe inner diameter on ε is not appreciable. From Eqs. (9) and (10), the effects of the pipe inner diameter and initial bubble size can be explained. By rearranging Eq. (10), the mass transfer coefficient is found to be proportional to $d_i^{-(1-0.86)}$ and the impact of the pipe inner diameter is therefore significantly reduced. Similarly, with some rearrangement of Eq. (9), R_2 therefore ε is greatly reduced with a smaller initial bubble size.

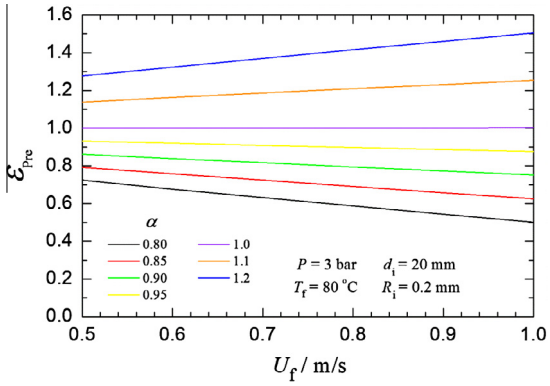

Fig. 13. Variation of predicted bubble size ratio with bulk liquid velocity for different saturation ratios.

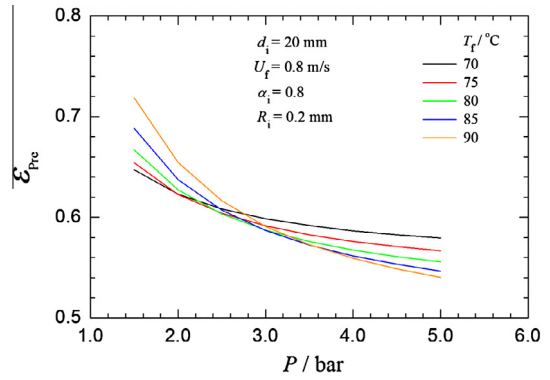

Fig. 14. Variation of predicted bubble size ratio with bulk liquid pressure for different bulk fluid temperatures.

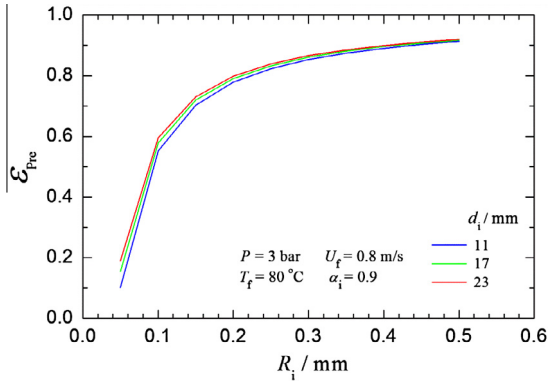

Fig. 15. Variation of predicted bubble size ratio with initial bubble radius for different inside diameters of pipe.

5. Conclusions

The measurements have been carried out for the dissolution of free bubbles in turbulent bubbly flow in under-saturated water conditions, the typical condition in a domestic wet central heating system. The bubble dissolution rates measured for the bubble size ratios are in the range of 1–12% per second or 0.65–18% per metre of horizontal pipe work with system conditions, hence increasing with a lower bulk fluid under saturation ratios and higher velocities. The dissolution mechanism is mainly dependent on the gas concentration in the bulk fluid flow and the degree of turbulence,

while the effects of the phase relative velocity, surface tension and bulk fluid temperature and pressure are considered to be negligible. The decrease in bubble size as it flows through the system pipe work is a result of the gas mass transfer from the bubble to the ambient liquid. The bubble dissolution model has been developed to consider the factors of fundamental bubble gas diffusion and the surrounding fluid turbulent flow. To precisely calculate the effect of turbulent diffusion, a new correlation of the Sherwood calculation was derived which ensures the model simulation are well matched to the measurements. With the help of the validated model, the gas bubble dissolution rates are greatly affected by operating and structure parameters such as fluid velocity, saturation ratio, velocity, temperature, pressure and initial bubble size. The effect of the pipe inner diameter, however, is minimal. Ultimately, the experimental and theoretical investigation on bubble dissolution in the central heating system is valuable for understanding bubble behaviours, and enabling an optimised location for the deaertor installation and overall improvement of system performance.

Acknowledgements

The authors would like to thank the Engineering and Physical Science Research Council (EPSRC), STEPS Malta, and Spirotech b v., the Netherlands, for supporting this research work.

References

[1] Joelsson A, Gustavsson L. District heating and energy efficiency in detached houses of differing size and construction. Appl Energy 2009;86:126–34.
[2] Chen X, Yang HX. Performance analysis of a proposed solar assisted ground coupled heat pump system. Appl Energy 2012;97:888–96.
[3] Wang JJ, Jing YY, Zhang CF, Zhai ZJ. Performance comparison of combined cooling heating and power system in different operation modes. Appl Energy 2011;88:4621–31.
[4] Fsadni AM, Ge YT, Lamers AG. Measurement of bubble detachment diameters from the surface of the boiler heat exchanger in a domestic central heating system. Appl Therm Eng 2011;31:2808–18.
[5] Kress TS, Keyes JJ. Liquid phase controlled mass transfer to bubbles in co-current turbulent pipeline flow. Chem Eng Sci 1973;28:1809–23.
[6] Lezhnin S, Eskin D, Leonenko Y, Vinogradov O. Dissolution of air bubbles in a turbulent water pipeline flow. Heat Mass Transfer 2003;39:483–7.
[7] Hesketh RP, Etchells AW, Fraser RTW. Experimental observations of bubble breakage in turbulent flow. Ind Eng Chem Res 1911;30:835–41.
[8] MartÍnez-Bazán C, Montas JL, Lasheras JC. On the breakup of an air bubble injected into fully developed turbulent flow: Part 1 – breakup frequency. J Fluid Mech 1999;401:157–82.
[9] Epstein PS, Plesset MS. On the stability of gas bubbles in liquid–gas solutions. J Chem Phys 1950;18:1505–9.
[10] Duda JL, Vrentas JS. Heat or mass transfer-controlled dissolution of an isolated sphere. Int J Heat Mass Transfer 1971;14:395–408.
[11] Cable M, Frade JR. The influence of surface tension on the diffusion-controlled growth or dissolution of spherical gas bubbles. Proc R Soc Lond 1988;420:247–65.
[12] Prodanovic V, Fraser D, Salcudean M. Bubble behaviour in sub cooled flow boiling of water at low pressures and low flow rates. Int J Multiphase Flow 2001;28:1–19.
[13] Akiyama M, Tachibana F. Motion of vapour bubbles in subcooled heated channel. Bull JSME 1974;17:241–7.
[14] Cable M. The dissolving of stationary gas bubbles in a liquid. Chem Eng Sci 1976;22:1393–8.
[15] Kentish S, Lee J, Davidson M, Ashokkumar M. The dissolution of a stationary spherical bubble beneath a flat plate. Chem Eng Sci 2006;61:7697–705.
[16] Yang WJ, Echigo R, Wotton DR, Hwang JB. Experimental studies of the dissolution of gas bubbles in whole blood and plasma – II. Moving bubbles or liquids. J Biomech 1967;22:1393–8.
[17] Semmens MJ, Ahmed T. Gas transfer from small spherical bubbles in natural and industrial systems. J Environ Syst 2003;29:101–23.
[18] Chen Q, Finney K, Li H, Zhang X, Zhou J, Sharifi V, et al. Condensing boiler applications in the process industry. Appl Energy 2012;89:30–6.
[19] Jones SF, Evans GM, Galvin KP. Bubble nucleation from gas cavities – a review. Adv Colloid Interface Sci 1999;80:27–50.
[20] Lubetkin S, Blackwell M. The nucleation of bubbles in supersaturated solutions. J Colloid Interface Sci 1988;26:610–5.
[21] Battino R. (Eds.). Nitrogen and air, solubility data series. Oxford: Pergamon Press; 1982 [10].
[22] Gerrard W. Solubility of gases and liquids. New York: Plenum Press; 1976.
[23] Image-Pro Plus Start-Up Guide. Media Cybernetics; 2010.
[24] Coleman HW, Steele WG. Experimentation and uncertainty analysis for engineers. 2nd ed. New York: John Wiley & Sons Inc.; 1999.
[25] Avdeev AA. Laws of growth, condensation and dissolution of vapor and gas bubbles in turbulent flows. High Temp 1988:214–20.
[26] Kawase Y, Halard B, Moo-Young MB. Theoretical prediction of volumetric mass transfer coefficients in bubble columns for Newtonian and non-Newtonian fluids. Chem Eng Sci 1987;42:1609–17.